Composition/Structural Evolution and Optical Properties of ZnO/Zn Nanoparticles by Laser Ablation in Liquid Media

Haibo Zeng, Weiping Cai,* Yue Li, Jinlian Hu, and Peisheng Liu

Key Laboratory of Materials Physics, Institute of Solid State Physics, Chinese Academia of Sciences, Hefei, 230031, P. R. China

Received: May 1, 2005; In Final Form: June 6, 2005

We present composition-controlled synthesis of ZnO−Zn composite nanoparticles by laser ablation of a zinc metal target in pure water or in aqueous solution of sodium dodecyl sulfate (SDS). By SDS concentration, composition and size of the nanoparticles can be controlled in a wide range. Relative amounts of the components Zn and ZnO, the particle size, and the microstructure can evolve with SDS concentration in solution. High SDS concentration corresponds to high relative amount of Zn nanoparticles existing as the core in the core/shell nanostructures, whereas low SDS concentration leads to high ZnO amount. This was explained by a dynamic mechanism on the basis of the competition between aqueous oxidation and SDS capping protection. Correspondingly, optical absorption spectra evolve from the excitonic peak of ZnO (about 350 nm) to the Zn surface plasmon resonance (about 242 nm) with rise of SDS concentration. A blue (about 450 nm) photoluminescence was observed in the obtained ZnO nanoparticles, which was attributed to existence of interstitial zinc in ZnO lattices. This study has revealed that laser ablation of active metal in liquid media is an appropriate method to synthesize a series of metal oxide semiconductor−metal composite nanoparticles with controlled composition and size.

1. Introduction

Fabrication of nanoparticles has been a focus of an ever-increasing number of researchers worldwide, mainly because of their unusual properties. These particulate materials find a vast range of applications in fabrication of new materials (such as ceramics, composites, etc.) and construction of micro- or nanodevices. Semiconductor−metal composite nanoparticles have been extensively studied for their attractive capability in improvement of catalytic and sensing properties[1−3] and tunable luminescence.[4]

Up to now, a large number of preparation methods are reported to produce nanoparticles, such as magnetic liquids,[5] metal−polymer nanocomposites,[6] semiconductors,[7] colloidal systems,[8] and so forth. Among them is the laser ablation technique, which was successfully developed as a gas-phase method for metallic and nonmetallic nanostructures.[9] Henglein and Cotton applied a pulsed laser to ablate pure metal targets in various solvents to form colloidal solutions.[10−12] Laser ablation of solids in liquid environment is a simple and versatile method to synthesize nanoparticles. The corresponding studies are mainly focused on two subjects: (i) preparation of nanoparticles via laser ablation of (mostly, noble) metal targets and[13−23] (ii) laser-induced modification of the size and shape of nanoparticles.[24−30] However, there have been few reports on the synthesis of nanoparticles using active main-group or transition-metal targets. Recently, several active metal oxides and hydroxides have successfully been synthesized.[31−35] In this case, strong reactions will take place in the aqueous solution, such as the reaction between water molecules with the ablated species, since the ablated active species are electronically excited and hence highly reactive; On the other hand, the effect of such aqueous oxidation should be controllable through surface modification by surfactant coverage and manipulation of laser parameters. Hereby, it is possible to obtain the metal oxide−metal composite nanoparticles by rapid reactive quenching with surfactant aqueous solution. Recently, we have successfully prepared ZnO−Zn nanoparticles with controllable composition and size by laser ablation of pure zinc metal in pure water or in aqueous solution of ionic surfactant. The optical absorption spectra exhibit an interesting evolution of two absorption peaks, located at 242 and 350 nm, respectively, with surfactant concentration. Photoluminescence (PL) measurements show an obvious blue emission which decreases sharply with the rise of surfactant concentration. The details are reported in this article.

2. Experimental Section

The typical experiment was carried out through pulsed laser ablation of a pure zinc plate in pure water or in aqueous solution of sodium dodecyl sulfate (SDS, 99.5%) surfactants with various concentrations from 0.0001 to 0.1 M. A zinc plate (99.99%) was fixed on the bracket in a glass vessel filled with 10 mL aqueous solution which was continuously stirred to disperse the smokelike colloids above the metal plate. The plate is located at 4 mm from the solution surface in the solution and then was ablated by the first harmonic (1064 nm) of a Nd:YAG laser operated at 10 Hz with a pulse width of 10 ns. A Scientech power meter monitors the output of the 1064-nm laser with the output of 70 mJ/pulse. The laser beam was focused on the metal plate with a spot size about 2 mm in diameter using a lens with a focal length of 150 mm. Laser ablation lasted for 30 min, and the solution gradually turned from brownish to yellow with the increase of ablation time. Most solutions became slightly turbid after the ablation. For the 0.01 M SDS solution, it was completely transparent and stable for more than 1 week without aggregation, and no obvious change of the corresponding optical

* Author to whom correspondence should be addressed. E-mail: wpcai@issp.ac.cn.

10.1021/jp052258n CCC: $30.25
Published on Web 09/10/2005

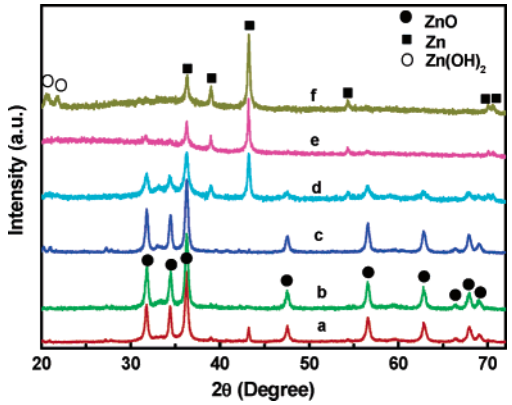

Figure 1. XRD patterns of the products prepared in pure water (a) and in surfactant solution with different SDS concentrations: 0.0001 M (b), 0.001 M (c), 0.01 M (d), 0.05 M (e), and 0.1 M (f). The pulse energy was fixed at 70 mJ.

spectrum was observed in 1 week after ablation, whereas the 0.05 M SDS solution was comparatively stable in 3 days. In other samples, there appear some floccules in several hours.

The optical absorption spectra of the obtained colloidal solutions were recorded, immediately after laser ablation (in about 5 min), by a Cary 5E UV−vis−IR spectrometer. Transmission electronic microscopic (TEM) examination was conducted on a transmission electronic microscope (JEM-200CX) by putting a drop of the sample solution on a carbon-coated copper grid. All of the colloidal suspensions were centrifuged at 4000 round/min, and the settled powders were characterized by X-ray diffraction (XRD) (the Philips X'Pert) using Cu Kα line (0.15419 nm). PL spectra and infrared (IR) spectra of the obtained powders were measured on the FLS920 PL spectrophotometer with a Xe lamp at room temperature and a NEXUS FT-IR spectrometer, respectively. The zeta potential of colloid particles was measured on Zetasizer 3000HS.

3. Results

Figure 1 shows XRD patterns of the products prepared in pure water and surfactant solutions with different SDS concentrations. The sample prepared in pure water exhibits strong diffraction peaks from ZnO and weak ones from pure Zn crystal, as shown in curve a in Figure 1. When the concentration of SDS is less than its critical micelle concentration (CMC, 0.008 M[28]), the products are composed of wurtzite ZnO, but no Zn is detected (see curves b and c in Figure 1). When SDS concentration is larger than the CMC, diffraction peaks of Zn crystal reappear and their intensity increases with the rise of SDS concentration, together with ever-decreasing ZnO peaks (see curves d and e in Figure 1). When the SDS concentration is up to 0.1 M, ZnO peaks disappear and $Zn(OH)_2$ peaks appear, in addition to the strong peaks from Zn crystal. These results demonstrate the component evolution of the products with SDS concentration. At low concentration (<CMC), the product is mainly composed of ZnO crystal. At moderate SDS concentration (0.01 M, near CMC), the products are mainly ZnO−Zn composite. After that, the main products are zinc crystals whose relative amount increases with the increase of SDS concentration. We can thus control the relative amount of ZnO and Zn crystals just by SDS concentration.

Figure 2 presents the TEM images corresponding to the samples shown in Figure 1. The products are composed of the particles with nearly spherical shape. For the samples prepared in SDS solution, the particles are covered with surfactant (especially for high SDS concentration). The corresponding particle size distributions and SDS concentration dependence of the mean sizes are shown in Figure 3. It can be seen that with the SDS concentration increasing, the size distribution width becomes narrow, and the mean size decreases rapidly from 44.5 to 18.1 nm except for an abnormal increase at 0.001 M. Further observation by high-resolution TEM has confirmed the

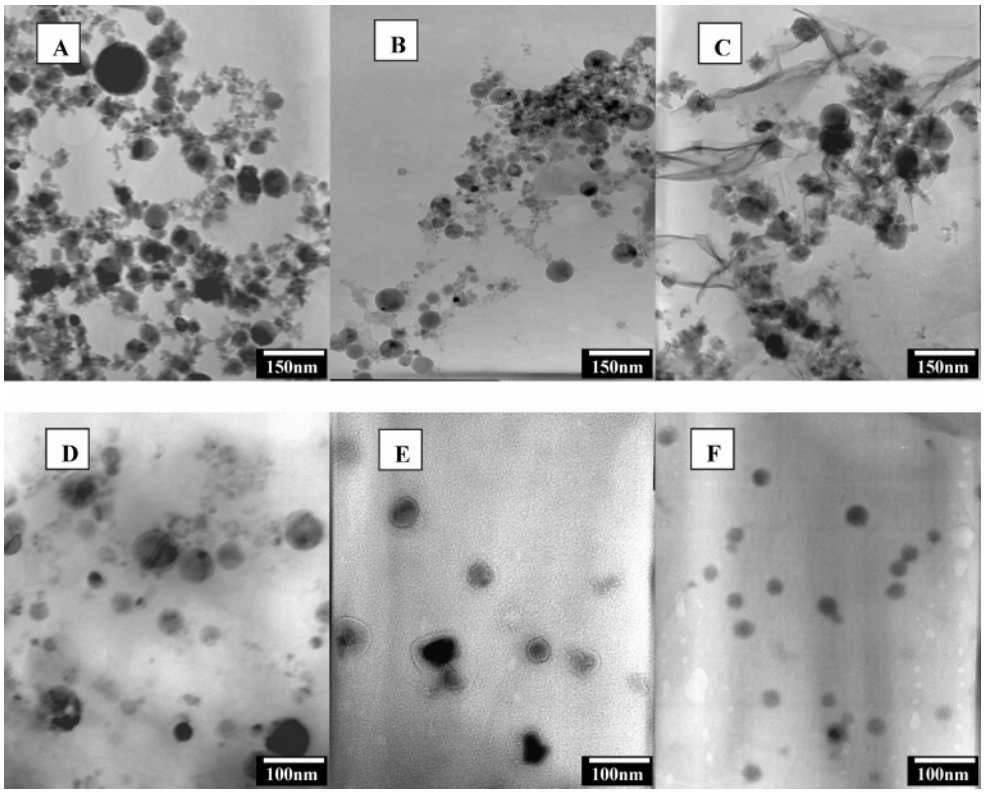

Figure 2. TEM images of samples prepared in aqueous solution with different SDS concentrations. A: 0.0 M (pure water), B: 0.0001 M, C: 0.001 M, D: 0.01 M, E: 0.05 M, and F: 0.1 M.

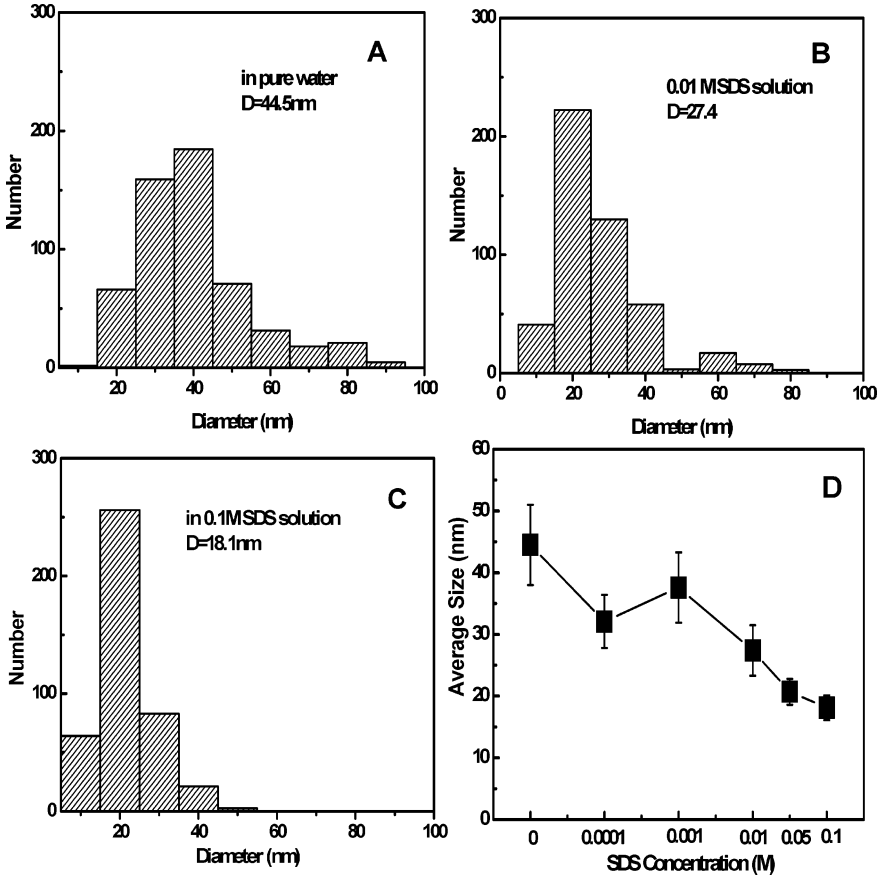

Figure 3. Particle size distribution of nanoparticles prepared in aqueous solution with different SDS concentrations. A: water, B: 0.01 M, C: 0.1 M, and D: SDS concentration dependence of the particle mean size.

existence of Zn/ZnO core/shell structured particles at the SDS concentration solution higher than 0.01 M, as shown in Figure 4. The lattice fringes well coincide with metal zinc and zinc oxide, respectively. The number of core/shell particles in the product increases with rise of SDS concentration from 0.01 M to 0.05 M.

Figure 5 shows the ultraviolet−visible (UV−vis) optical absorption spectra of the colloidal suspension of different samples in aqueous solution with and without SDS. Obviously, there are two absorption peaks at about 350 and 242 nm corresponding to two concentration ranges of SDS, respectively. For the sample prepared in pure water, there is an absorption peak at 350 nm, which decreases with the increase of SDS concentration up to 0.001 M. However, when the SDS concentration is about 0.03 M, the peak at 350 nm vanishes, and another peak at 242 nm appears and increases with further increase of the SDS concentration.When the SDS concentration is near its CMC (0.005 and 0.01 M), the absorption peak at 350 nm is replaced by a shoulder and the UV absorption band is uplifted sharply, which behaves as a transition between the two absorption peaks. In addition, the absorption of pure SDS aqueous solution is very weak in the wavelength region studied (see curve j in Figure 5). Therefore, the absorption peaks originate from the nanoparticles suspended in the solution.

Figure 6 shows the FT-IR spectra collected from the nanoparticles mulled in KBr wafer. There is a strong band at 460 cm^{-1} for all samples, which is associated with the characteristic vibration mode of Zn−O bonds.[31] The broad absorption peak centered at 3445 cm^{-1} corresponds to the −OH groups and water molecules.[36] The bands at 1061, 1468, 2849, 2920, and 2952 cm^{-1} are attributed to −C−H stretching and bending modes,[37] respectively. The band at 1228 cm^{-1} is related to $-SO_4$ of SDS molecules.[37] The absorption peak belonging to Zn−O bonds decreases with the increase of SDS concentration, whereas the absorption peak corresponding to surfactant molecules increases, which indirectly confirms that the ZnO relative amount reduces with increase of the SDS. The FT-IR measurements coincide well with the XRD results.

Figure 7 shows the PL spectra of ZnO−Zn composite nanoparticles whose main component is ZnO because of the lower SDS concentration. There is an emission peak in the blue region, which decreases sharply with the SDS concentration (see the inset of Figure 7) together with a slight red-shift from 443 nm for the sample without SDS to 460 nm for the sample prepared with 0.005 M SDS. In a common case, the PL emission of ZnO includes the characteristic exciton or interband transition emission in UV range[38] and the defect emissions located in green or yellow range associated with oxygen vacancies.[38] Interestingly, in our experiments, an obvious blue-emission band centered around 450 nm (2.75 eV) was observed.

4. Discussion

4.1. Formation and Structural Morphology of Nanoparticles. Laser ablation in active liquid medium is of particular interest because of its high nonequilibrium processing which allows synthesis of novel phases of materials.[35,39] Although the fundamental mechanism regarding nanostructure formation by laser ablation in liquid is still not fully understood, according to previous studies of laser ablation at liquid−solid interface, interaction between pulsed laser light and the target can create local high-temperature and high-pressure plasma plumes above the target surface. Tetsuo Sakka and co-workers[40−47] have investigated the time evolution of the plasma plume induced

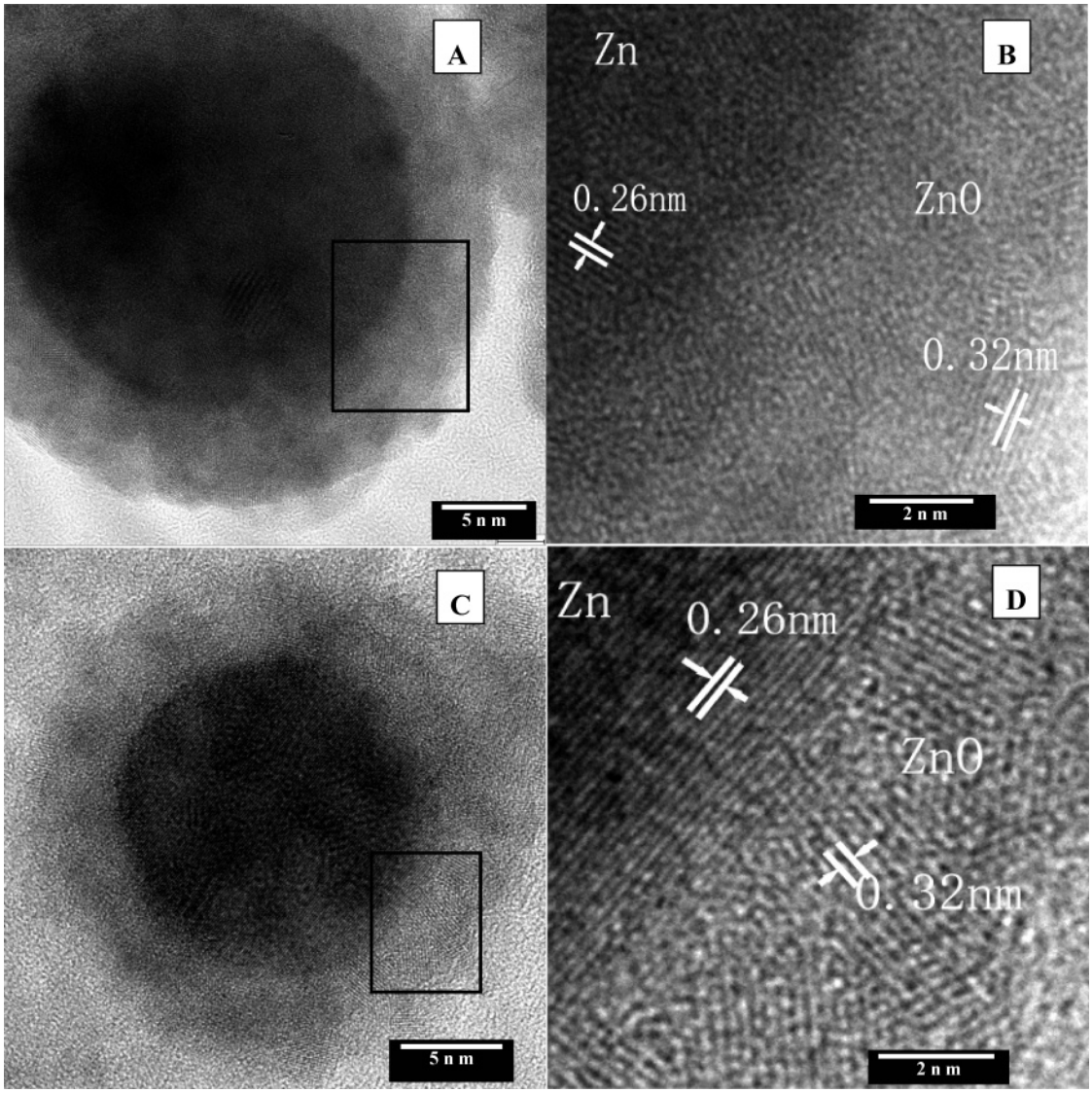

Figure 4. HRTEM images of typical nanoparticles in the samples from 0.01 M (A, B) and 0.05 M (C, D) SDS solutions; images B and D are the local magnified images corresponding to the frame regions marked in images A and C, respectively.

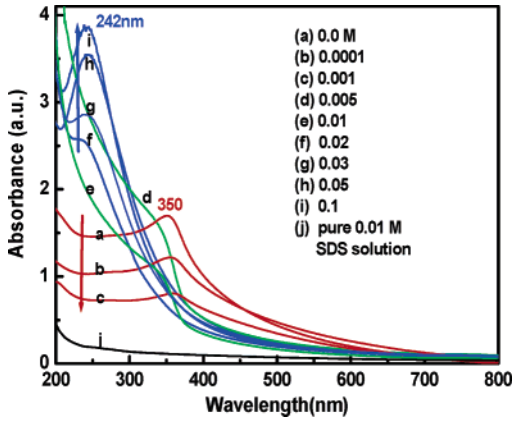

Figure 5. Optical absorption spectra of the colloidal solution produced by laser ablation of a zinc plate in aqueous solution with different SDS concentrations. The spectra of pure SDS solution with different concentrations are of no obvious difference except the slight increase of the background with SDS.

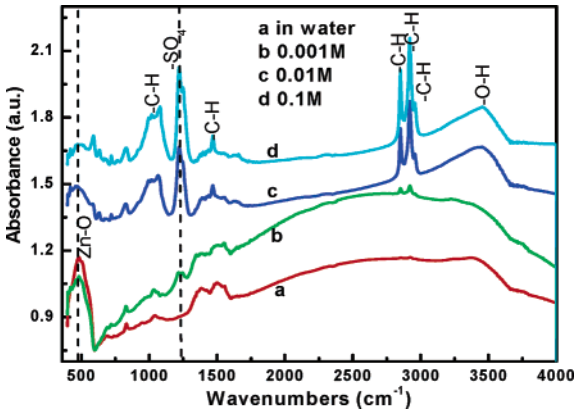

Figure 6. Fourier transform infrared (FT-IR) spectra of KBr wafers containing nanoparticles from colloidal solution with different SDS concentrations.

by laser ablation of graphite in water with a Q-switch Nd:YAG laser of 70 mJ/pulse. By emission spectra detection and theoretical simulation, it was found that the pressure can be as high as 1 GPa and the carbon atomic density as high as 10^{21} cm^{-3}, and more importantly, the plasma plume was formed in about 59 ns after the interaction between the laser and the target, and its temperature was up to 6000 K and started to decrease in about 1000 ns.[43] Various chemical reactions and physical processes will thus take place among the ablated metal species, solvent molecules, and surfactant molecules, which induces the

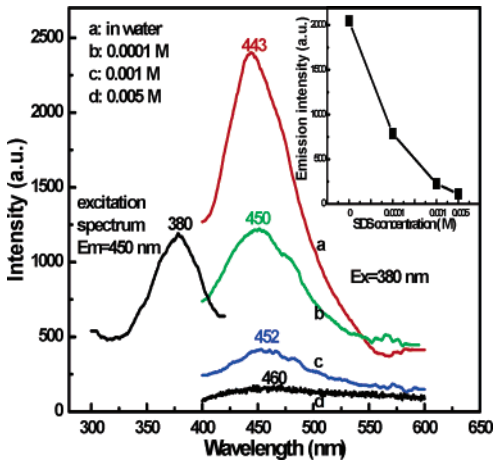

Figure 7. Room-temperature PL spectra and excitation spectrum for the samples prepared with different SDS concentrations: (a) 0.0 M, (b) 0.0001 M, (c) 0.001 M, (d) 0.005 M. (Ex = 380 nm, Em = 450 nm). The inset: the surfactant concentration dependence of the emission intensity.

formation of nanoparticles in solution. The structure, morphology, size, and hence properties of nanoparticles will differ for different media including solvent and surfactant. So, the properties of nanoparticles can be controlled by solution composition

On the basis of that mentioned above and of our experimental results, the formation of ZnO−Zn composite nanoparticles could be described in three steps, as illustrated in Scheme 1. (I) The high-temperature and high-pressure zinc plasma (without solvent) is produced in the solid−liquid interface quickly after the interaction between pulsed laser and the metal target. (II) The subsequent ultrasonic and adiabatic expansion[40,43−45] of the high-temperature and high-pressure zinc plasma leads to cooling of the zinc plume region and hence to formation of zinc clusters. In our case, the interval between two successive pulses [or one pulse (10 ns) and its subsequent break] is 0.1 s (10 Hz), which is much longer than the life of the plasma plume. Therefore, the next laser pulse has no interaction with the former plasma plume. (III) With the extinguishment of the plasma, the formed zinc clusters encounter the solvent and surfactant molecules in the solution, which induces some chemical reactions and capping effects. The final structure and morphology of the particles are dependent on the SDS concentration in solution or on the competition between aqueous oxidation of zinc particles and SDS protection.

According to the above proposed formation mechanism, when the SDS protection effect is minor or the SDS concentration is very low [C < CMC (C denotes the SDS concentration in solution)], the aqueous oxidation effect will be dominant because of the highly active Zn clusters formed in step II, leading to the formation of the initial oxidation product $Zn(OH)_2$ which can easily be decomposed to ZnO on the basis of the reactions

$$Zn_{(clusters)} + 2H_2O = Zn(OH)_2 + H_2 \quad (1)$$

$$Zn(OH)_2 = ZnO + H_2O \quad (2)$$

The existence of a small amount of metal zinc in the final product in pure water is due to the incomplete oxidation for some larger Zn particles formed in step II, leading to Zn/ZnO core/shell structured composite nanoparticles. A small amount of SDS will restrain aggregation (or growth) of Zn clusters after extinguishment of plasma (see the following text) and will lead to full oxidation of the particles. So, the final products are almost ZnO (see curves b and c in Figure 1) without Zn. However, when C > CMC, the protection of SDS becomes dominant with further increasing of SDS concentration, because the SDS molecules will form a bilayer and even surface micelles on the particle surface,[14,15,46,47] which decreases significantly the oxidation rate. The product from 0.01 M SDS solution is the typical ZnO−Zn nanocomposits, in which the relative amount of ZnO and Zn is comparative. For the typical particles (large enough size), a Zn/ZnO core/shell structure will be formed (see Figure 4), while for the smaller particles, only a ZnO structure is formed because of full oxidation. With the SDS concentration increasing to 0.05 M solution, the ZnO relative amount reduces sharply, the ZnO shell thickness of core−shell nanoparticles decreases, but the number of core−shell particles in the product increases. When the concentration is up to 0.1 M (about 10 times of CMC), we obtain the metal Zn nanoparticles covered with very thin $Zn(OH)_2$ and almost undetectable ZnO, which indicates that both

SCHEME 1. Illustration of the Formation Process for ZnO/Zn Composite Nanoparticles[a]

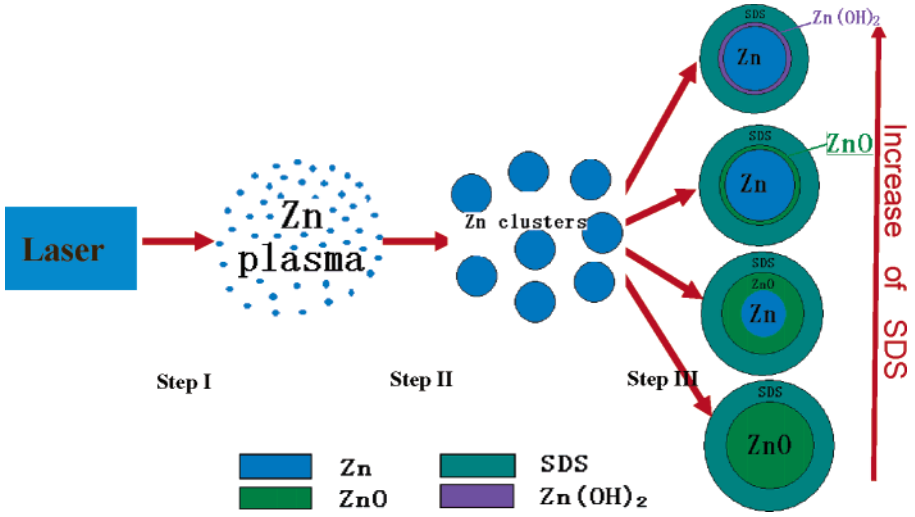

[a] For details, see the text. Step I: Production of high-temperature and high-pressure zinc plasma above the metal target quickly after one pulse shot. Step II: Subsequent ultrasonic and adiabatic expansion of the plasma leads to cooling of the zinc plume region and hence to formation of zinc clusters. Step III: Formation of final particles with different morphologies and structures during extinguishment of the plasma, depending on the SDS concentration in solution (the direction of the arrow at the most right: increase of SDS concentration in solution).

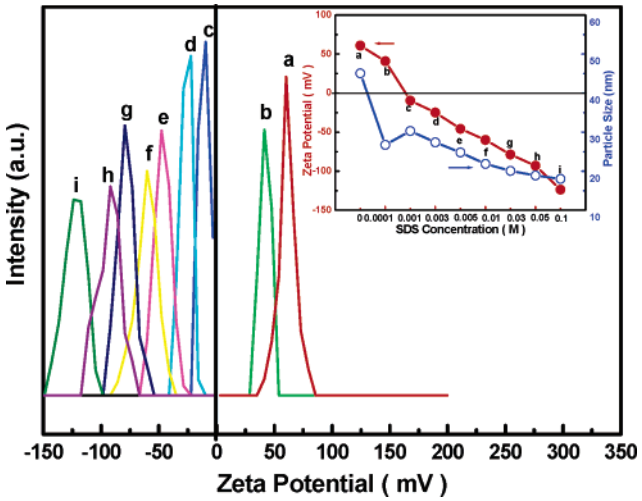

Figure 8. Zeta potential of colloidal particles from different SDS concentration solutions. Curves a−i correspond to the samples prepared with SDS concentration shown in the inset. The inset: Zeta potentials (○) and particle sizes (●) versus SDS concentration.

oxidation and dehydration have been depressed intensively in this extreme situation. Step III in Scheme 1 schematically exhibits such structural evolution of the typical core/shell composite nanoparticles with SDS concentration.

The decrease of nanoparticle size with the increase of SDS concentration in solution can be attributed to space separation effect of SDS capping and electrostatic repulsive force among colloidal particles, as previously reported.[15] The higher SDS concentration leads to the higher surface coverage of SDS molecules on the particle surface and to the stronger space separation effect, inducing formation of smaller particles. On the other hand, the surface charge on the formed particles also changes with SDS concentration, leading to different interaction between particles. The surface of ZnO nanoparticles in pure water is usually positively charged because the pH value of the solution (about 7.0) is below the isoelectric point of ZnO (about 9.3).[48] The negatively charged $C_{12}H_{25}SO_4$ (DS^-) ions would preferably attach on the particle surface by electrostatic force. At 0.001 M SDS solution, the particle surface becomes nearly neutral because of the neutralization between DS^- ions and the surface positive charge. At higher concentration, the surface of ZnO nanoparticles is negatively charged contrarily because of the excessive adsorption of DS^- ions. The electrostatic repulsive force between particles emerges again and increases with a rise in SDS concentration. The abnormal increase of particle size at 0.001 M SDS solution (see Figure 3D) can be attributed to the decrease of electrostatic repulsive force because of such reversion of surface-charged property.

Further experiment has confirmed such evolution of surface-charged property of particles by measurement of the zeta potential of colloidal particles from different SDS concentration solution, as indicated in Figure 8. The particles in pure water or 0.0001 M SDS solution are positively charged, and the charge density decreases with the rise of SDS concentration. Assuredly, the reversion of charged property occurs at the concentration between 0.0001 M and 0.001 M (see inset of Figure 8). The particles in 0.001 M SDS solution are slightly negatively charged. When the concentration of SDS is larger than 0.001 M, the surface negative charge density increases with the rise of SDS concentration, corresponding to ever-decreasing particle size (see the inset in Figure 8). This reveals the charge-dominated effect on the particle size.

4.2. Optical Absorption Peaks in the UV Region. As demonstrated in Figure 5, the ZnO−Zn colloidal solution shows successively two absorption peaks at 350 and 242 nm, respectively, with increase of SDS concentration. However, these two peaks hardly shift with the SDS concentration. Therefore, they should have different origins. When SDS concentration is less than 0.005 M, the main product is ZnO. Obviously, the peak at 350 nm can be attributed to the exciton absorption of ZnO particles, although it is not of obvious position shift because of the particles' much larger size than the Bohr radius of ZnO (1.8 nm), as previously reported.[49] The depression of the exciton peak is associated with SDS, which needs further work.

When SDS concentration is higher than 0.01 M, Zn metal is dominant in the product and hence ZnO exciton peak disappears. Although there are very few reports on the zinc surface plasmon reasonance (SPR), recently, Lee and co-workers have reported the zinc SPR absorption in 255 nm of Zn nanocrystals embedded in a SiO_2 matrix.[50] We suggest that the peak at 242 nm comes from the SPR absorption of zinc nanoparticles in the SDS aqueous solution. In fact, there are several metals whose SPR is located in the range of 200−300 nm, such as In, Mg, Cr, Pd, Cd, and so forth.[51,52] With an increase of SDS concentration, the Zn amount increases and the SPR at 242 nm is enhanced.

When the SDS concentration is 0.005∼0.01 M, the transitional absorption shoulder appears, which needs further work to reveal its origin. Since the corresponding product consists of Zn and ZnO in comparable amounts, such a shoulder could be associated with the coupling result of exciton absorption and metal interband absorption. The UV absorption is uplifted sharply because of the transition of interband electrons in metal zinc.

4.3. Blue Photoluminescence. There are some reports on the weak blue emission of ZnO nanostructures, including ZnO nanotubes,[53] ZnO clusters inside mesoporous silica,[54] and ZnO nanorods.[55] However, the mechanism of this emission is not clear yet. Fu and co-workers have calculated the energy level of various defect centers, such as vacancies of oxygen and zinc, interstitial oxygen and zinc, and antisite oxygen in bulk ZnO (band gap 3.36 eV).[56] The gap between conduction band and level of oxygen vacancies is 2.28 eV (about 540 nm) and that from interstitial zinc level to valence band is 2.9 eV (about 425 nm). The former was well consistent with the normal green emission of ZnO. The blue emission in this study could be attributed to interstitial zinc in ZnO nanoparticles. It is reasonable that there exists interstitial zinc in ZnO lattices, since the rapid and nonequilibrium formation of nanoparticles from zinc plasma plume is induced by laser ablation in liquid. The depression and slight red-shift of the blue emission with SDS concentration rise can be attributed to the SDS capping-induced surface passivation on ZnO particles. This is similar to the ZnO nanoparticles capped with PVP[40] or with amphoteric surfactant LDA,[33] which can eliminate the trap or defect states.

5. Summary

We demonstrated the feasibility of controlled-synthesis of ZnO−Zn composite nanoparticles by laser ablation of pure active zinc target in liquid media. Laser ablation of the target induces local zinc plasma above the target, which results in the formation of Zn clusters during extinguishment of the zinc plasma plume, and subsequent aqueous oxidation can lead to the formation of ZnO nanoparticles. However, SDS can depress such oxidation because of its surface capping on the particles and can lead to the formation of Zn/ZnO core/shell nanoparticles. Relative amounts of components Zn and ZnO can thus

evolve with SDS concentration in solution. High SDS concentration corresponds to high relative amount of Zn nanoparticles, whereas low SDS concentration leads to high ZnO amount. Correspondingly, optical absorption spectra evolve from the excitonic peak of ZnO to the Zn SPR with rise of SDS concentration. The space separation effects of SDS capping and electrostatic repulsive force among colloidal particles result in the decrease of nanoparticle size. Blue PL can be attributed to existence of interstitial zinc in ZnO lattices because of the rapid and nonequilibrum process.

We believe that laser ablation of active metal in liquid media is an appropriate method to synthesize a series of metal oxide semiconductor−metal composite nanoparticles with controlled composition and size, which is of importance to study the catalysis, sensitivity, and energy conversion of metal−semiconductor nanocomposites.

Acknowledgment. This work was supported by the National Natural Science Foundation of China (grant numbers: 50271069 and 10474099).

References and Notes

(1) Subramanian, V.; Wolf, E.; Kamat, P. V. *J. Phys. Chem. B* **2001**, *105*, 11439.
(2) Cozzoli, P. D.; Comparelli, R.; Fanizza, E.; Curri, M. L.; Agostiano, A.; Laub, D. *J. Am. Chem. Soc*. **2004**, *126*, 3868.
(3) Dawson, A.; Kamat, P. V. *J. Phys. Chem. B* **2001**, *105*, 960.
(4) Hsu, Y. J.; Lu, S. Y. *Langmuir* **2004**, *20*, 23.
(5) Shafi, K. P. V. M.; Wizel, S.; Prozorov, T.; Gedanken, A. *Thin Solid Films* **1998**, *318*, 38.
(6) Gubin, S. P.; Kosobudskii, J. D. *Russ. Chem. Rev.* **1983**, *52*, 776.
(7) Shi, J.; Golder, S.; Babcock, K.; Awschalom, D. D. *Science* **1996**, *271*, 937.
(8) Henglein, A. *J. Phys. Chem*. **1993**, *97*, 5457.
(9) Morales, A. M.; Lieber, C. M. *Science* **1998**, *279*, 208.
(10) Fojtik, A.; Henglein, A. *Ber. Bunsen-Ges. Phys. Chem.* **1993**, *97*, 252.
(11) Neddersen, J.; Chumanov, G.; Cotton, T. M. *Appl. Spectrosc.* **1993**, *47*, 1959.
(12) Sibbald, M. S.; Chumanov, G.; Cotton, T. M. *J. Phys. Chem.* **1996**, *100*, 4672.
(13) Pyatenko, A.; Shimokawa, K.; Yamaguchi, M.; Nishimura, O.; Suzuki, M. *Appl. Phys. A* **2004**, *79*, 803.
(14) Mafune, F.; Kohno, J. Y.; Takeda, Y.; Kondow, T. *J. Phys. Chem. B* **2000**, *35*, 8335.
(15) Mafune, F.; Kohno, J. Y.; Takeda, Y.; Kondow, T. *J. Phys. Chem. B* **2000**, *104*, 9111.
(16) Mafune, F.; Kohno, J. Y.; Takeda, Y.; Kondow, T. *J. Phys. Chem. B* **2001**, *105*, 5114.
(17) Mafune, F.; Kohno, J. Y.; Takeda, Y.; Kondow, T. *J. Phys. Chem. B* **2002**, *31*, 7577.
(18) Mafune, F.; Kohno, J. Y.; Takeda, Y.; Kondow, T. *J. Phys. Chem. B* **2003**, *107*, 4218.
(19) Takeuchi, Y.; Ida, T.; Kimura, K. *J. Phys. Chem. B* **1997**, *101*, 1322.
(20) Sylvestre, J. P.; Kabashin, A. V.; Sacher, E.; Meunier, M.; Luong, J. H. *J. Am. Chem. Soc*. **2004**, *126*, 7176.
(21) Chen, Y. H.; Yeh, C. S. *Chem. Commun*. **2001**, 371.
(22) Tsa, S. H.; Liu, Y. H.; Wu, P. L.; Yeh, C. S. *J. Mater. Chem*. **2003**, *13*, 978.
(23) Pyatenko, A.; Shimokawa, K.; Yamaguchi, M.; Nishimura, O.; Suzuki, M. *Appl. Phys. A* **2004**, *79*, 803.
(24) Mafune, F.; Kohno, J. Y.; Takeda, Y.; Kondow, T. *J. Phys. Chem. B* **2001**, *105*, 9050.
(25) Mafune, F.; Kohno, J. Y.; Takeda, Y.; Kondow, T. *J. Am. Chem. Soc*. **2003**, *125*, 1686.
(26) Satoh, N.; Hasegawa, H.; Tsujii, K.; Kimura, K. *J. Phys. Chem. B* **1994**, *98*, 2143.
(27) Aguirre, C. M.; Moran, C. E.; Young, J. F.; Halas, N. J. *J. Phys. Chem. B* **2004**, *108*, 7040.
(28) Link, S.; Burda, C.; Nikoobakht, B.; Sayed, M. A. E. *J. Phys. Chem. B* **2000**, *104*, 6152.
(29) Bosbach, J.; Martin, D.; Stietz, F.; Wenzel, T.; Trager, F. *Appl. Phys. Lett.* **1999**, *74*, 2605.
(30) Tsujia, T.; Watanabeb, N.; Tsuji, M. *Appl. Surf. Sci.* **2003**, *211*, 189.
(31) Liang, C. H.; Shimizu, Y.; Sasaki, T.; Koshizaki, N. *J. Phys. Chem. B* **2003**, *107*, 9220.
(32) Liang, C. H.; Shimizu, Y.; Masuda, M.; Sasaki, T.; Koshizaki, N. *Chem. Mater.* **2004**, *16*, 963.
(33) Usui, H.; Shimizu, Y.; Sasaki, T.; Koshizaki, N. *J. Phys. Chem. B* **2005**, *109* (1), 120.
(34) Zhang, C. Y.; Zhong, X. L.; Wang, J. B.; Yang, G. W. *Chem. Phys. Lett*. **2003**, *370*, 522.
(35) Rosen, M. J. *Surfactants and Interfacial Phenomena*, 2nd ed.; Wiley-Interscience: New York, 1989.
(36) Clearfield, A.; Kieke, M.; Kwan, J.; Colon, J. L.; Wang, R. C. *J. Inclusion Phenom. Mol. Recongnit. Chem.* **1991**, *11*, 361.
(37) Vanheusden, K.; Warren, W. L.; Seager, C. H.; Tallant, D. R.; Voigt, J. A.; Gnade, B. E. *J. Appl. Phys*. **1996**, *79*, 7983.
(38) Ogale, S. B.; Patil, P. P.; Phase, D. M.; Bhandarkar, Y. V.; Kulkarli, S. K.; Kulkarli, S.; Ghaisas, S. V.; Kanetkar, S. M.; Bhide, V. G.; Guha, S. *Phys. Rev. B* **1987**, *36*, 8237.
(39) Cozzoli, P. D.; Curri, M. L.; Agostiano, A.; Leo, G.; Lomascolo, M. *J. Phys. Chem. B* **2003**, *107*, 4756.
(40) Zhu, S.; Lu, Y. F.; Hong, M. H.; Chen, X. Y. *J. Appl. Phys*. **2001**, *89*, 2400.
(41) Saito, K.; Sakka, T.; Ogata, Y. *J. Appl. Phys*. **2003**, *94*, 5530.
(42) Sakka, T.; Iwanaga, S.; Ogata, Y. H.; Matsunawa, A.; Takemoto, T. *J. Chem. Phys*. **2000**, *112*, 8645.
(43) Kim, D.; Lee, H. *J. Appl. Phys*. **2001**, *89*, 5703.
(44) Zhu, S.; Lu, Y. F.; Hong, M. H. *Appl. Phys. Lett.* **2001**, *79*, 1396.
(45) Berthe, L.; Fabbro, R.; Peyre, P.; Tollier, L.; Bartinicki, E. *J. Appl. Phys*. **1997**, *82*, 2826.
(46) Matijevic, E.; Ottewill, R. H. *J. Colloid Sci.* **1958**, *13*, 242.
(47) Esumi, K. *J. Colloid Interface Sci.* **2001**, *241*, 1.
(48) Kooli, F.; Chsem, I. C.; Vucelic, W. *Chem. Mater*. **1996**, *8*, 1969.
(49) Wong, E. M.; Searson, P. C. *Appl. Phys. Lett*. **1999**, *74*, 2939.
(50) Lee, J. K.; Tewell, C. R.; Schulze, R. K.; Nastasi, M.; Hamby, D. W.; Lucca, D. A.; Jung, H. S.; Hong, K. S. *Appl. Phys. Lett*. **2005**, *86*, 183111.
(51) Creighton, A.; Eadon, D. G. *J. Chem. Soc., Faraday. Trans*. **1991**, *87*, 3881.
(52) Zhang, X. H.; Xie, S. Y.; Jiang, Z. Y.; Zhang, X.; Tian, Z. Q.; Xie, Z. X.; Huang, R. B.; Zheng, L. S. *J. Phys. Chem. B* **2003**, *107*, 10114.
(53) Zhang, W. H.; Shi, J. L.; Wang, L. Z.; Yan, D. S. *Chem. Mater*. **2000**, *12*, 1408.
(54) Wu, J. J.; Liu, S. C. *Adv. Mater*. **2002**, *14*, 215.
(55) Lin, B. X.; Fu, Z. X.; Jia, Y. B. *Appl. Phys. Lett*. **2001**, *79*, 943.
(56) Guo, L.; Yang, S. H.; Yang, C. L.; Yu, P.; Wang, J. N.; Ge, W. K.; George, K.; Wong, L. *Chem. Mater*. **2000**, *12*, 2268.